ACS APPLIED MATERIALS & INTERFACES

Research Article

www.acsami.org

Lignin-Derived Fused Electrospun Carbon Fibrous Mats as High Performance Anode Materials for Lithium Ion Batteries

Su-Xi Wang,[†] Liping Yang,[‡] Ludger Paul Stubbs,[‡] Xu Li,*[,†,§] and Chaobin He*[,†,∥]

[†]Institute of Materials Research and Engineering, A*STAR (Agency for Science, Technology and Research), 3 Research Link, Singapore 117602

[‡]Institute of Chemical and Engineering Sciences, A*STAR (Agency for Science, Technology and Research), 1 Pesek Road, Jurong Island, Singapore 627833

[§]Department of Chemistry, National University of Singapore, 3 Science Drive 3, Singapore 117543

[∥]Department of Materials Science and Engineering, National University of Singapore, 9 Engineering Drive 1, Singapore 117576

Supporting Information

ABSTRACT: A novel biomass-based nitrogen-doped free-standing fused carbon fibrous mat was fabricated from lignin–polyethylene oxide (PEO) (90:10) blend via electrospinning followed by carbonization and thermal annealing in the presence of urea. The morphology and structure of the carbon fibers were characterized by field-emission scanning electron microscopy, Raman spectroscopy, X-ray photoelectron spectroscopy, and elemental analysis, and their electrochemical properties were investigated for the first time as anode in lithium ion batteries (LIBs). The fused carbon fibers without nitrogen doping exhibited high specific capacity up to 445 mA h g^{-1} at a current density of 30 mA g^{-1} (comparable to polyacrylonitrile (PAN) derived carbon nanofibers) and good cyclic stability at different current rates. After thermal annealing in the presence of urea, the charge capacity was further improved to as high as 576 mA h g^{-1} and still maintained a good capacity of about 200 mAh g^{-1} even at a high current rate of 2000 mA g^{-1}. This research demonstrates the great promise of lignin-derived nanocarbon materials for applications in energy storage systems.

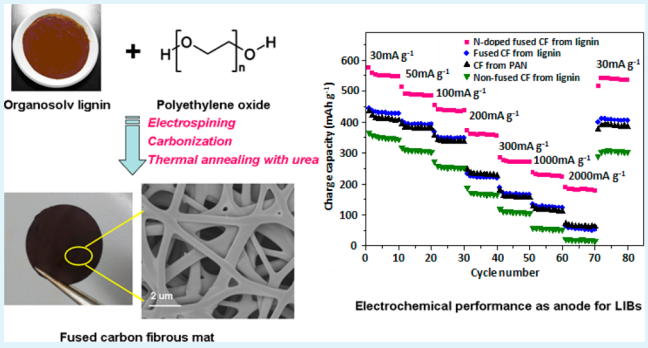

KEYWORDS: *lignin, carbon fiber, electrospinning, free-standing, nitrogen doping, lithium ion batteries*

1. INTRODUCTION

Nowadays, in a world subjected to severe shortage of resources and various environmental problems, there is an increasing pressure for almost every manufacturer to go "green" and seek sustainable development, especially for the energy industry that is highly dependent on fossil fuel resources. Rechargeable lithium-ion batteries (LIBs) have been the most efficient and environmentally benign energy storage devices and are being widely utilized in various portable electronic devices, hybrid electric vehicles, and emerging smart grids.[1−4] For the electrodes in LIBs, carbon materials have been holding the predominant position and demonstrated to be the most prospective for industrialization because of their low cost, easy accessibility, and processability.[5] However, the already commercialized graphite suffers from rather low energy density (theoretical capacity 372 mA h g^{-1}) as the anode material for LIBs. The newly developed nanocarbon materials (such as graphene, carbon nanotubes, mesoporous carbons, carbon nanofibers, etc.) exhibit much higher performance as electrode materials for energy storage devices because of their high conductivity and accessible specific surface area.[6,7] However, the nonrenewability and high cost of the carbon precursors (such as coals, petroleum, polyacrylonitrile (PAN), phenolic resins, etc.) as well as the complex manufacturing processes restrain their large-scale application. Energy shortages and growing market demands still drive us to find cost-effective and inexhaustible sources for producing high performance nanocarbon materials.

Nature provides a wide variety of renewable raw materials with diverse properties and chemical compositions. The potential of sustainable biomass-derived carbons for energy application is being well recognized nowadays. As an example, Li et al. have reported that mesoporous nitrogen-rich carbons derived from egg protein show a reversible lithium storage capacity of 1780 mA h g^{-1}.[8] Although a vast variety of biomass source such as husk rice,[9] peanut shells,[10] sugar,[11] olive and cherry stones,[12] etc. have been demonstrated to be promising candidates for producing carbon electrode materials for lithium ion batteries, most of the derived carbons are not free-standing and some are fabricated from tedious and complicated process.

Received: May 22, 2013
Accepted: November 20, 2013
Published: November 20, 2013

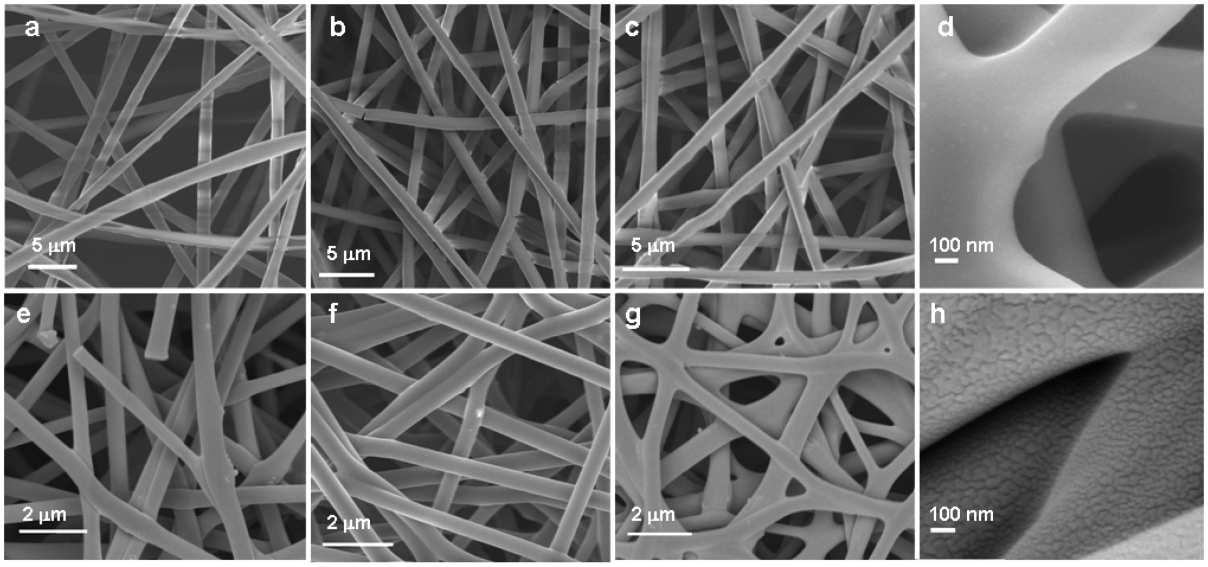

Figure 1. FESEM images of electrospun nanofibers from lignin−PEO blends with lignin to PEO ratio of (a) 97:3, (b) 95:5, and (c) 90:10. FESEM images of electrospun carbon nanofibers derived from lignin−PEO blends with lignin to PEO ratio of (e) 97:3, (f) 95:5, and (g) 90:10. High resolution FESEM images show the surface of the carbon fibers (d) without and (h) with nitrogen doping.

Lignin, the second most abundant polymer in nature, is considered to be the largest biomass source of aromatic functionality with high carbon content above 60%, making it the most attractive sustainable precursor for carbonaceous materials. However, in spite of its high production of over 50 million tons annually, the utilization of lignin-derived carbon is rather limited except for some applications as chars or activated carbons for water or air purification.[13] Over the past decade, there has been an explosion of research interest in enabling the conversion of lignin into high-value chemicals or materials, and the biggest challenge of the task is the variable structure and composition of lignin with regard to different isolation processes and plant resources. One of the newly explored applications for lignin/lignin derivatives is to be utilized in electrochemical devices.[14,15] However, in those protocols, lignin was only used as an additive (with weight ratio no more than 50%) to form composite electrode materials and the lignin employed was limited to a certain type.

Electrospinning is a most straightforward and powerful method for generating continuous nanofibers from solutions of polymers or polymer blends.[16,17] Lignin has been previously utilized as inexpensive feedstock for producing general purpose carbon fibers with size ranging from 20 to 80 μm through conversional melt spinning,[18−24] and lignin-based electrospun nanofibers (with diameters less than 1 μm) have been developed only very recently.[25−29] Our group has been actively developing carbon nanomaterials for energy-related applications in the past few years,[30−33] and thus, we have keen interest in converting this low-cost and renewable biomass to electrospun carbon nanofibers as electrode materials for energy storage devices. This is because (1) electrospun carbon fibers can form highly porous free-standing mats that could be directly used as electrode materials accessible to electrolyte ions without adding any conductive agent or binder, largely simplifying the fabrication process, and (2) the performance of the carbon nanofibers could be further improved by incorporating heteroatoms via simple post-treatment. In this report, we present a straightforward method to fabricate N-doped free-standing fused carbon fibrous mats from lignin−polyethylene oxide (PEO) blend via electrospinning followed by carbonization and thermal annealing with urea. The morphology and structure of the lignin-derived carbon nanofibers were studied, and their electrochemical properties as anode for lithium ion batteries were investigated for the first time. The results demonstrate the great promise of carbon fibrous mat derived from low cost, abundant, and renewable lignin for applications in energy storage systems.

2. EXPERIMENTAL SECTION

2.1. Materials. Organosolv (Alcell) lignin was purchased from BOC Sciences (USA) and dried under vacuum before use. Polyethylene oxide (PEO, M_w = 600K, Sigma Aldrich), urea (Alfa Aesar), polyacrylonitrile (PAN, M_w = 150K, International Laboratory USA), and *N*,*N*-dimethylformamide (DMF, Alfa Aesar) were used as received.

2.2. Preparation of Fused Electrospun Carbon Fibrous Mats from Lignin. In a typical experiment, 436 mg of Alcell lignin and 48 mg of PEO were dispersed into 2 mL of DMF under magnetic stirring and the suspension was heated at 60 °C for 3 h. After cooling to room temperature naturally under continuous stirring, the solution was placed in a 1 mL plastic syringe fitted with a flap tip 22 G needle and was electrospun using a horizontal electrospinning setup. Typically, electrospinning was performed at 6.5−7.0 kV with a feeding rate of 1 mL/h, and the needle tip-to-plate substrate distance was 10 cm. The nanofibers were collected on aluminum foil and dried at 70 °C under vacuum overnight. The dried nanofibers were thermostabilized in a tube furnace under atmospheric environment. The temperature was ramped from 25 to 200 °C at 1 °C min^{-1} and kept at 200 °C for 2 h. The stabilized fibers were then heated from 200 to 900 °C at 10 °C min^{-1} under a flow of argon (150 cm^3 STP/min) and carbonized at 900 °C for 2 h.

2.3. Preparation of N-Doped Carbon Fibrous Mats from Lignin. In a typical procedure, an amount of 20 mg of lignin-derived fused carbon fibrous mats (carbonized at 500 °C for 2 h) was immersed in 10 mL of 10 % urea aqueous solution and then dried under vacuum for several hours. The resulting mixture was heated from 25 to 900 °C at 5 °C min^{-1} and kept at 900 °C for 2 h. After the mixture was cooled to room temperature, the obtained N-doped carbon fibrous mats were washed with deionized water and dried at 60 °C under vacuum overnight.

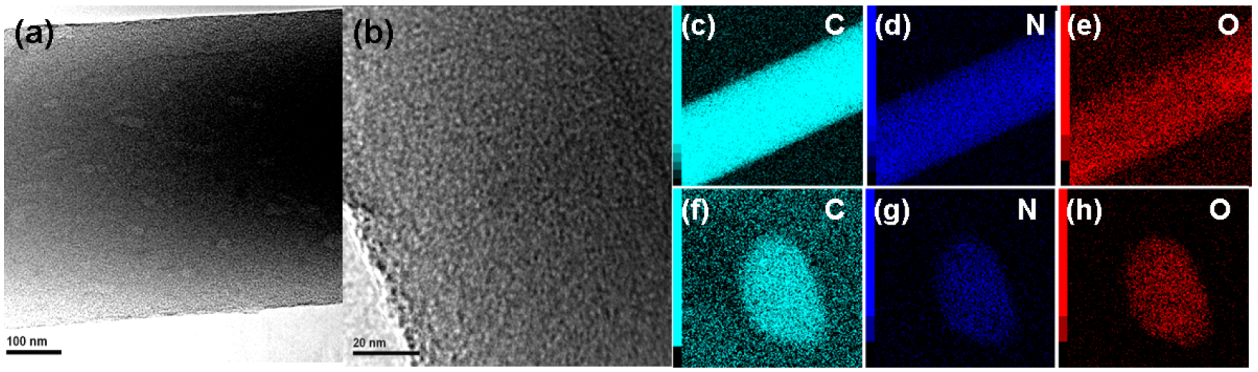

Figure 2. High resolution TEM images of N-doped carbon fibers at different magnification (a, b). Normal EDX mapping of N-doped carbon fibers: (c) C element, (d) N element, and (e) O element. Cross-sectional EDX mapping of the N-doped carbon fibers: (f) C element, (g) N element, and (h) O element.

2.4. Structural Characterization. Morphology of the nanofibers were observed under JEOL JSM 6700 field-emission scanning electron microscope at an accelerating voltage of 5 kV. All samples were coated with a thin gold layer before SEM imaging. High resolution TEM and the corresponding EDX mapping images of the N-doped carbon fibers were obtained with a JEOL 2100 transmission electron microscope. The carbon fibers were dispersed into ethanol using ultrasonication followed by casting onto copper grids. To observe the cross-sectional morphology, the N-doped carbon fibers were embedded into epoxy and cut into 50 nm slices using a microtome (Leica) before attaching onto copper grids. The surface chemistry of the samples was studied by X-ray photoelectron spectroscopy (XPS) analysis which was conducted on a VG ESCA LAB-220i XL X-ray photoelectron spectrometer with an exciting source of Al. Elemental analysis was performed on an elemental analyzer (EA, flash 1112 series), and Raman spectra were recorded on a Jobin Yvon T64000 triple spectrograph micro-Raman system. N_2 adsorption/desorption isotherms at 77 K were measured using a Micromeritics ASAP 2020 system. The electrical conductivity of the carbon fibrous mats was measured by a four-point probe method on the Microxact automated probe station at room temperature.

2.5. Electrochemical Measurements. The electrochemical performance was tested with the lignin-derived carbon fibrous mats, lithium foil, and 1 M $LiPF_6$ in ethylene carbonate/dimethyl carbonate (1:1 v/v ratio) as the working electrode, counter electrode, and electrolyte, respectively. All were assembled into 2032 button cells in an argon-filled glovebox with moisture and oxygen levels of less than 1 ppm. The galvanostatic charge/discharge tests were performed using a NEWARE battery tester at different current densities with a cutoff voltage window of 0.005−3.0 V. The cyclic voltammetry test was performed on an electrochemical workstation (PGSTAT302, Autolab) within a voltage window of 0−3.0 V and at a scan rate of 0.01 V s^{-1}. The electrochemical impedance spectroscopy (EIS) study was conducted using the same electrochemical workstation in a frequency range of 10^6 to 10^{-2} Hz and at an ac amplitude of 5 mV.

3. RESULTS AND DISCUSSION

The preferred lignin used in this research was organosolv lignin, which contains very small amounts of inorganic components, and this method could be extended to other technical lignins as well. The lignin-derived electrospun nanofibers were fabricated from electrospinning the solutions of organosolv lignin and PEO in DMF. The addition of PEO could greatly improve the viscosity and spinnability of the solution, and the weight ratio of lignin to PEO could be tuned from 99:1 to 80:20 by varying the concentration of the polymer solution from 35 to 20 wt %. Parts a−c of Figure 1 present the typical SEM images of the smooth, bead-free nanofibers from lignin−PEO with diameters of ∼1 μm. The as-spun fibers were then stabilized in the air by heating from room temperature to 200 °C at 1 °C min^{-1} and subsequently carbonized under argon at 900 °C to generate carbon nanofibers with diameters of ∼500 nm. Notably, it was observed that high proportions of PEO (≥10%) resulted in fusion among the adjacent carbon fibers (as shown in Figure 1g), which could be ascribed to the strong melting behavior of PEO (mp 66−70 °C) during heat treatment. Compared to the separated carbon fibers (as shown in Figure 1e and Figure 1f), the interconnected fiber webs will provide shorter and more continuous pathways for electron transportation and thus reduce the electrochemical resistance of the electrode. The electrical conductivity of the nonfused carbon fibers and fused carbon fibers is 7.34 and 10.53 S/cm, respectively.

Doping with heteroatoms (such as N, B) has proven to be an enabling strategy to improve electrochemical reactivity and electrical conductivity of carbonaceous materials.[34−38] To further increase the electrochemical performance of the lignin-derived carbon fibers, we managed to dope nitrogen into the above fused carbon fibers through thermal annealing with urea. In order to obtain N-doped carbon fibrous mats tough enough to be punched to free-standing electrode materials, an extra carbonization process at a low temperature of 500 °C is required (see Figure S1 in Supporting Information) to preform "soft" carbon fiber mats with good mechanical strength, which were subsequently vacuum impregnated with urea aqueous solution and subjected to a second carbonization at 900 °C to realize nitrogen doping and higher degree of graphitization. The content of nitrogen can be tuned by varying the concentration of the urea solution and could reach as high as 12.6 wt % as revealed by elemental analysis. The high magnification FESEM images in Figure 1d and Figure 1h represent the surface of the carbon fibers before and after nitrogen doping, respectively. The formation of cracks on the carbon fibers after doping with nitrogen is mainly due to the emission of ammonia gas that was generated from the decomposition of molten urea at high temperature. The resulting N-doped carbon fibrous mats are still tough enough to be punched to free-standing electrode. Parts a and b of Figure 2 present the high-resolution transmission electron microscopy (HRTEM) images of the N-doped carbon fibers, which reveal defects and large quantities of micropores within the fibers. Furthermore, both the normal and cross-sectional EDX mapping images (Figure 2c−e and Figure 2f−h) demonstrate the uniform distribution of the nitrogen, carbon, and oxygen elements in the carbon fibers. Nitrogen-doped fused carbon fibers with nitrogen content of 12.6 wt % showed

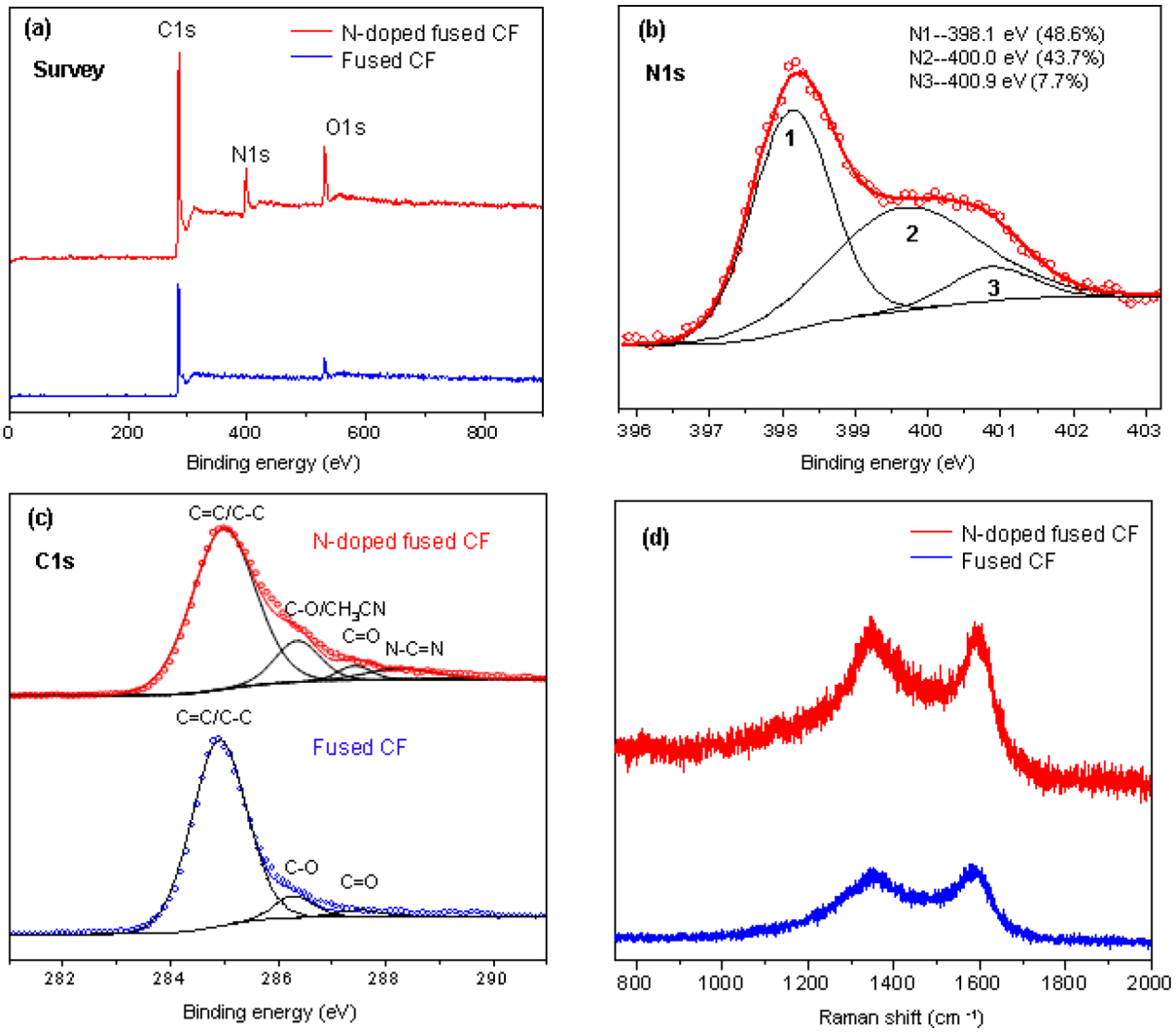

Figure 3. XPS of lignin-derived fused carbon fibers with and without N-doping: (a) survey; (b) N1s; (c) C1s. (d) Raman spectra of the fused carbon fibers (carbonized at 900 °C) with and without nitrogen doping.

higher electrical conductivity (12.24 S/cm) than non-nitrogen-doped fused carbon fibers (10.53 S/cm).

X-ray photoelectron spectroscopy (XPS) analysis was conducted to study the elemental composition and chemical states of the elements that exist in the fused electrospun carbon fibers with and without nitrogen doping. Figure 3a displays the survey spectrum (0−900 V) of the two samples, which basically includes C1s, O1s, and N1s (only for the N-doped ones) without any other impurities, and the total elements' atomic ratios are summarized in Table 1. As shown in Figure 3b, the N1s spectrum can be fitted into three component peaks located at 398.1, 400.0, and 400.9 eV, which are identified to pyridinic nitrogen, pyrrolic nitrogen, and quaternary nitrogen, respectively.[36,37] Furthermore, the order of the corresponding proportions of the nitrogen species is as follows: pyridinic nitrogen (48.6%) > pyrrolic nitrogen (43.7%) > quaternary nitrogen (7.7%). As reported previously, only pentagonal pyrrolic nitrogen is formed at low temperature of around 300 °C and it could be converted to pyridinic and quaternary nitrogen as the carbonization temperature rises.[36,38] The C1s spectra ranging from 281 to 291 eV of the two samples are shown in Figure 3c. For the fused carbon fibers without nitrogen doping, the spectrum could be fitted into three obvious peaks centered at 284.9, 286.3, and 287.6 eV, which could be assigned to sp^2 C═C/sp^3 C−C (89.8%), C−O (7.7%), and C═O (2.5%) bonds, respectively. After doping with nitrogen, the peak area proportion of the C−C bonds (centered at 285.0 eV) decreases to 76.6%. And the peaks corresponding to CH_3CN/C−O (13.7%), C═O (3.3%), and N−C═N (6.4%) are observed at 286.3, 287.4, and 288.1 eV, respectively.[39]

Table 1. XPS Peak Analysis of the Carbon Fibers from Lignin

sample	C (at. %)	O (at. %)	N (at. %)
fused carbon fibers	89.11	10.89	
N-doped fused carbon fibers	76.85	9.94	13.21

The Raman spectra of the fused carbon fibers from lignin before and after N-doping are shown in Figure 3d. The peak intensity ratio of the D band (1350 cm^{-1}, amorphous carbon) to G band (1580 cm^{-1}, graphitic carbon) increased from 1.32 to 1.51 after high temperature annealing with urea, indicating that nitrogen doping introduces a large amount of topological defects and structural disorder to the carbon fibers. Compared to the peak positions of the carbon fibers before N-doping, red

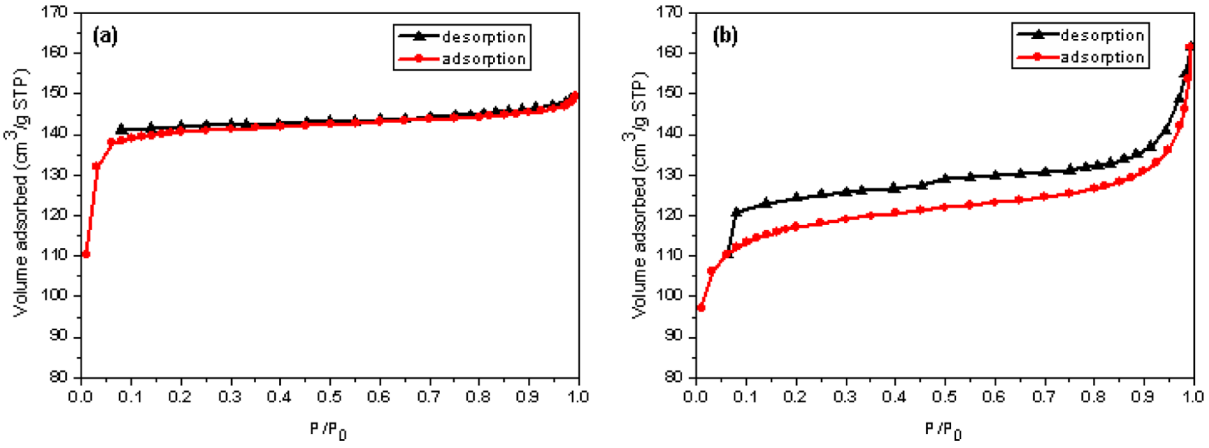

Figure 4. Nitrogen adsorption/desorption isotherms of the fused carbon fibers without (a) and with (b) nitrogen doping.

shift was observed with both the D-band (from 1350.8 to 1347.7 cm^{-1}) and G-band (from 1593.8 to 1586.7 cm^{-1}) of the carbon fibers after N-doping. Many factors can affect the Raman peak positions of carbonaceous materials, such as doping, layer numbers, defects, strains, substrate, etc.[40] Here, the downshift of both the D-band and G-band could be ascribed to doping with nitrogen, which introduces more defects and causes a change in vibration energy levels. Similar results were also observed with N-doped graphene and carbon nanotubes.[40,41]

Furthermore, the specific surface area and porous structure of the carbon fibers were studied by N_2 adsorption−desorption analysis at 77 K. Figure 4 shows the isotherms of the lignin-derived fused carbon fibers with or without nitrogen doping, and all the porous structure parameters are summarized in Table 2. Both isotherms of the carbon samples could be classified as type I, revealing a microporous structure with the gas adsorption volume quickly reaching saturation at low pressure region (P/P_0 < 0.1) due to monolayer adsorption of N_2 molecules inside the pores. The pure carbon sample has a BET surface area of 473 m^2 g^{-1} and a microporosity ratio as high as 87% with an average pore size of 2.6 nm. Nitrogen doping through thermal annealing with urea resulted in a decrease in the S_{BET} (381 m^2 g^{-1}) and the microporosity (57%). The relatively lower surface area and total pore volume could be ascribed to unification of the micropores rather than creation of more micropores at the fiber surface. The steep uptake at a relative pressure of 0.9−1.0 and the existence of a hysteresis loop in the isotherm after nitrogen doping demonstrate the increase of the meso-macroporous structure.

Table 2. Porous Structure Parameters for Lignin-Derived Carbon Fibers

sample	S_{BET} (m^2 g^{-1})[a]	V_t (cm^3g^{-1})[b]	V_m (cm^3g^{-1})[c]	APW (nm)[d]
fused carbon fibers	473	0.31	0.27	2.6
N-doped fused carbon fibers	381	0.28	0.16	5.9

[a]S_{BET}: BET surface area. [b]V_t: total pore volume measured at P/P_0 = 0.99. [c]V_m: pore volume of micropore (pore size of <2 nm). [d]APW: adsorption average pore width (4 V/A by BET).

The electrochemical properties of the lignin-derived carbon fibers were further investigated as anode for LIBs. Figure 5a shows the initial charge/discharge curves of the lignin-derived carbon fibrous mats at a current density of 30 mA g^{-1}. Compared with the non-fused carbon fibers (fabricated from lignin−PEO blend with a weight ratio of 97 to 3) which have an initial charge capacity of 365 mA h g^{-1}, the fused carbon fibers (fabricated from lignin−PEO blend with a weight ratio of 90:10) exhibit a superior capacity of 445 mA h g^{-1}, which is comparable with that of electrospun carbon nanofibers from PAN (~450 mA h g^{-1}) and far exceeds that of graphite (~320 mA h g^{-1}) under the same testing conditions.[42] An even higher charge capacity of 576 mA h g^{-1} is observed after doping the fused carbon fibers with nitrogen. All three samples exhibit similar initial discharge capacities around 650 mA h g^{-1}; however, the corresponding initial columbic efficiency of the N-doped carbon fibers is 82.8 %, much higher than those of the carbon samples without nitrogen (56.2% for nonfused carbon fibers and 68.2 % for fused ones). In the initial discharge curves, the nonfused and fused carbon fibers without nitrogen doping show an obvious plateau at ~1.2 V, which is not observed in the curve of the N-doped ones. The voltage plateau is attributed to the rapid formation of SEI (solid electrolyte interphase) during the first discharge caused by the electrolyte decomposition, contributing to the higher irreversible capacity and lower columbic efficiencies of the two carbon samples.[43,44] This can be verified with the cyclic voltammograms of the three carbon samples at the first scanning cycle (Figure 5b). Compared to the N-doped carbon fibers which exhibit a lithium intercalation peak starting from 1.0 V, the other two carbon samples show much bigger and broader intercalation peaks starting from 1.2 and 1.5 V with fused carbon fibers and nonfused carbon fibers, respectively. These results suggest that modification of carbon materials with heteroatoms could hinder the SEI formation and reduce the initial capacity loss with high columbic efficiency.

The rate capacities of the lignin-derived carbon samples were measured by conducting charge−discharge cycles at different current densities, with that of the PAN-based electrospun carbon fibers (fabricated according to the reported procedure[42]) as a comparison. As shown in Figure 5c, the fused carbon fibrous mats derived from lignin exhibit almost the same Li^+-ion storage capacity and cyclic stability as the carbon fibers from PAN at each current density from 30 to 2000 mA g^{-1}. Notably, the fused carbon fibers with nitrogen doping exhibit much higher capacities at each stage. Even at a very high current density of 2000 mA g^{-1}, a satisfying capacity value of ~200 mA h g^{-1} is still achieved with the N-doped carbon fibers.

dx.doi.org/10.1021/am4043867 | ACS Appl. Mater. Interfaces 2013, 5, 12275−12282

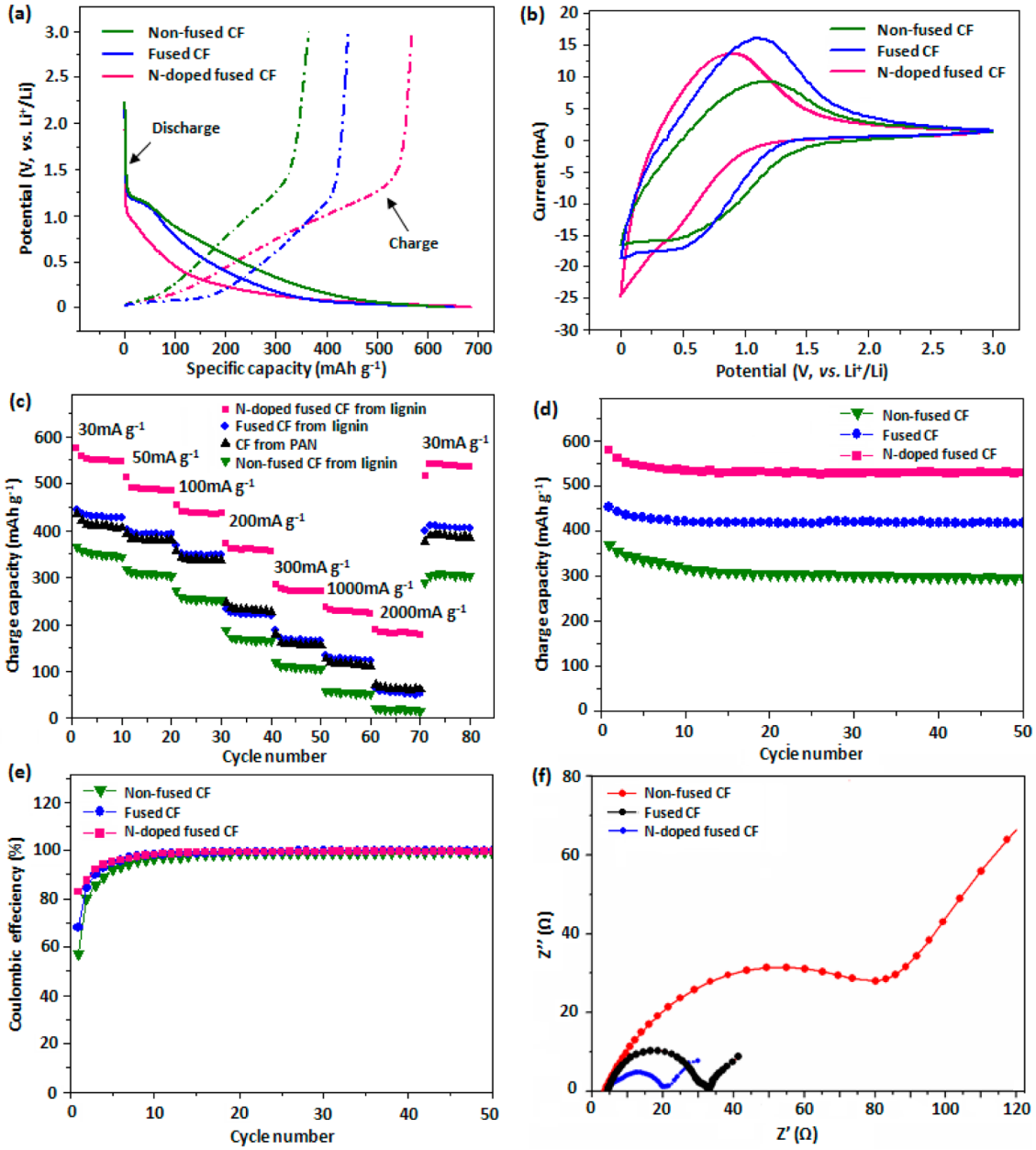

Figure 5. (a) Initial discharge−charge curves of the lignin-derived nonfused carbon fibers, fused carbon fibers, and N-doped fused carbon fibers at a current rate of 30 mA g^{-1}. (b) Cyclic voltammogram of the lignin-derived carbon fibers at the first cycle. The voltage window and scanning rate are 3.0−0.0 V and 0.01 V s^{-1}, respectively. (c) Charge capacities of the carbon samples at different current rates. (d) Cyclic performance and (e) corresponding Coulombic efficiency of the lignin-derived carbon fiber electrodes cycled at a current density of 30 mA g^{-1}. (f) Electrochemical impedance spectroscopy (EIS) of the lignin-derived carbon fibers before charging−discharging testing.

When the current density is tuned back to 30 mA g^{-1} after cycling at different rates, the specific capacities of the lignin-derived carbon fibers can be almost recovered to the original value. Figure 5d displays the cyclic stability of the carbon samples evaluated at a current density of 30 mA g^{-1} up to 50 cycles, and the corresponding Coulombic efficiencies are shown in Figure 5e. Although the charge capacities decrease obviously during the first three cycles, the fused carbon fibers before and after nitrogen doping still retained 92.7% and 91.8 % of the initial capacitance after 50 cycles, respectively. Furthermore, high Coulombic efficiencies (>99%) were observed with all the three carbon samples after 20 cycles. Although cracks were observed on the N-doped carbon fibers (Figure 1h), their morphology and the fibrous geometry were well maintained after the cycling test (Figures S4 and S5) except for a layer of SEI formed on the surface which led to the capacity fading. The good electrochemical stability and high degree of reversibility again highlight the great promise of the materials for practical applications.

To better understand the differences in electrochemical performances of the three kinds of carbon fibers from lignin, electrochemical impedance spectroscopy (EIS) study was also conducted before charge−discharge test. As represented in Figure 5f, all the impedance plots show a depressed semicircle in the high to middle frequency region, which is assigned to the charge-transfer impedance at the electrolyte/electrode interface, and an inclined line with ~45° slope in the middle to low frequency region which is related to the Li diffusion process

dx.doi.org/10.1021/am4043867 | ACS Appl. Mater. Interfaces 2013, 5, 12275−12282

within the carbonaceous electrode.[45] As shown in the figure, the fused carbon fibers exhibit much lower interfacial resistance as well as charge transfer resistance compared to that of the nonfused ones, which could be attributed to better electrical contact and easier electron/ion transfer within the fused fiber webs. The electrochemical resistance is further decreased remarkably after doping nitrogen into the carbon fibers, which can enhance the reactivity and facilitate electron transportation, thus promoting the electrochemical performance.

4. CONCLUSION

Lignin has been utilized as a sustainable precursor for fabricating free-standing carbon fibrous mats as high performance anode materials for lithium ion batteries via conventional electrospinning technique and thermal treatment process. Fused carbon fibers obtained through incorporation of certain proportions of low-melting-point polymer additive exhibit much lower electrical resistance as well as good electrochemical performance (with specific capacity up to 445 mA h g^{-1}), which is comparable to that of PAN-derived carbon fibers. Doping with nitrogen can further improve their specific capacity as well as electrochemical conductivity effectively. The fabrication process is economical and straightforward and can be conducted in large-scale production. This research demonstrates the great promise of lignin-derived nanocarbon materials for applications in energy storage systems and also opens up new possibilities for converting inexpensive biomass to high-value carbonaceous materials.

■ ASSOCIATED CONTENT

Ⓢ Supporting Information

Preparation of the N-doped carbon fibers; fused carbon fibers from lignin with two stages of carbonization; microstructure of N-doped carbon fibers after cycling test. This material is available free of charge via the Internet at http://pubs.acs.org.

■ AUTHOR INFORMATION

Corresponding Authors

*X.L.: phone, +65 68748421; e-mail, x-li@imre.a-star.edu.sg.
*C.H.: phone, +65 68748145; e-mail, cb-he@imre.a-star.edu.sg or msehc@nus.edu.sg.

Notes

The authors declare no competing financial interest.

■ ACKNOWLEDGMENTS

The authors acknowledge the financial support from the Agency for Science, Technology and Research (A*STAR, Singapore), Project 1124004040.

■ REFERENCES

(1) Tarascon, J. M.; Armand, M. *Nature* **2001**, *414*, 359−367.
(2) Bruce, P. G.; Scrosti, B.; Tarascon, J. M. *Angew. Chem., Int. Ed.* **2008**, *47*, 2930−2946.
(3) Palacin, M. R. *Chem. Soc. Rev.* **2009**, *38*, 2565−2575.
(4) Jeong, G.; Kim, Y. U.; Kim, H.; Kim, Y. J.; Sohn, H. J. *Energy Environ. Sci.* **2011**, *4*, 1986−2002.
(5) Novak, P.; Goers, D.; Spahr, M. E. *Carbons for Electrochemical Energy Storage and Conversion Systems*; CRC Press: Boca Raton, FL, 2009; pp 236−328.
(6) Xin, S.; Guo, Y.-G.; Wan, L.-J. *Acc. Chem. Res.* **2012**, *45*, 1759−1769.
(7) Nishihara, H.; Kyotani, T. *Adv. Mater.* **2012**, *24*, 4473−4498.
(8) Li, Z.; Xu, Z.; Tan, X.; Wang, H.; Holt, C. M. B.; Stephenson, T.; Olsen, B. C.; Mitlin, D. *Energy Environ. Sci.* **2013**, *6*, 871−878.
(9) Zhang, F.; Wang, K. X.; Li, D. G.; Chen, J. S. *Electrochem. Commun.* **2009**, *11*, 130−133.
(10) Fey, G. T.; Lee, D. C.; Lin, Y. Y.; Kumar, T. P. *Synth. Met.* **2003**, *139*, 71−80.
(11) Xing, W.; Xue, J. S.; Dahn, J. R. *J. Electrochem. Soc.* **1996**, *143*, 3046−3052.
(12) Caballero, A.; Hernan, L.; Morales, J. *ChemSusChem* **2011**, *4*, 658−663.
(13) Suhas; Carrott, P. J. M.; Ribeiro Carrott, M. M. L. *Bioresour. Technol.* **2007**, *98*, 2301−2312.
(14) Milczarek, G.; Inganas, O. *Science* **2012**, *335*, 1468−1471.
(15) Abe, H.; Hakozaki, M. Method for Producing Lignin from Which Organic Acid Is Removed and Lead Storage Battery Obtained by Adding Lignin from Which Organic Acid Is Removed to Negative Electrode Active Substance. JP 2006169134, 2006.
(16) Greiner, A.; Wendorff, J. H. *Angew. Chem., Int. Ed.* **2007**, *46*, 5670−5703.
(17) Reneker, D. H.; Yarin, A. L. *Polymer* **2008**, *49*, 2387−2425.
(18) Sudo, K.; Shimizu, K. *J. Appl. Polym. Sci.* **1998**, *44*, 127−134.
(19) Kubo, S.; Uraki, Y.; Sano, Y. *Carbon* **1998**, *36*, 1119−1124.
(20) Kadla, J. F.; Kubo, S.; Venditti, R. A.; Gilbert, R. D.; Compere, A. L.; Griffith, W. *Carbon* **2002**, *40*, 2913−2920.
(21) Kubo, S.; Kadla, J. F. *Macromolecules* **2004**, *37*, 6904−6911.
(22) Kubo, S.; Kadla, J. F. *J. Polym. Environ.* **2005**, *13*, 97−105.
(23) Qin, W.; Kadla, J. F. *Ind. Eng. Chem. Res.* **2011**, *50*, 12548−12555.
(24) Baker, D. A.; Gallego, N. C.; Baker, F. S. *J. Appl. Polym. Sci.* **2012**, *124*, 227−234.
(25) Lallave, M.; Bedia, J.; Ruiz-Rosas, R.; Rodriguez-Mirasol, J.; Cordero, T.; Otero, J. C.; Marquez, M.; Barrero, A.; Loscertales, I. G. *Adv. Mater.* **2007**, *19*, 4292−4296.
(26) Ruiz-Rosas, R.; Bedia, J.; Lallave, M.; Loscertales, I. G.; Barrero, A.; Rodriguez-Mirasol, J.; Cordero, T. *Carbon* **2010**, *48*, 696−705.
(27) Dallmeyer, I.; Ko, F.; Kadla, J. F. *J. Wood Chem. Technol.* **2010**, *30*, 315−329.
(28) Seo, D. K.; Jeun, J. P.; Kim, H. B.; Kang, P. H. *Rev. Adv. Mater. Sci.* **2011**, *28*, 31−34.
(29) Ago, M.; Okajima, K.; Jakes, J. E.; Park, S.; Rojas, O. J. *Biomacromolecules* **2012**, *13*, 918−926.
(30) Kong, J.; Liu, Z.; Yang, Z.; Tan, H. R.; Xiong, S.; Wong, S. Y.; Li, X.; Lu, X. *Nanoscale* **2012**, *4*, 525−530.
(31) Kong, J.; Tan, H. R.; Tan, S. Y.; Li, F.; Wong, S. Y.; Li, X.; Lu, X. *Chem. Commun.* **2010**, *46*, 8773−8775.
(32) Kong, J.; Wong, S. Y.; Zhang, Y.; Tan, H. R.; Li, X.; Lu, X. *J. Mater. Chem.* **2011**, *21*, 15928−15934.
(33) Yang, Z.-C.; Zhang, Y.; Kong, J.-H.; Wong, S. Y.; Li, X.; Wang, J. *Chem. Mater.* **2013**, *25*, 704−710.
(34) Qie, L.; Chen, W.-M.; Wang, Z.-H.; Shao, Q.-G.; Li, X.; Yuan, L.-X.; Hu, X.-L.; Zhang, W.-X.; Huang, Y.-H. *Adv. Mater.* **2012**, *24*, 2047−2050.
(35) Wu, Z. S.; Ren, W.; Xu, L.; Li, F.; Cheng, H. M. *ACS Nano* **2011**, *5*, 5463−5471.
(36) Su, F.; Poh, C. K.; Chen, J. S.; Xu, G.; Wang, D.; Li, Q.; Lin, J.; Lou, X. W. *Energy Environ. Sci.* **2011**, *4*, 717−724.
(37) Chen, X. Y.; Xie, D. H.; Chen, C.; Liu, J. W. *J. Colloid Interface Sci.* **2013**, *393*, 241−248.
(38) Mou, Z.; Chen, X.; Du, Y.; Wang, X.; Yang, P.; Wang, S. *Appl. Surf. Sci.* **2011**, *258*, 1704−1710.
(39) Pevida, C.; Drage, T. C.; Snape, C. E. *Carbon* **2008**, *46*, 1464−1474.
(40) Wei, D.; Liu, Y.; Wang, Y.; Zhang, H.; Huang, L.; Yu, G. *Nano Lett.* **2009**, *9*, 1752−1758.
(41) Keskar, G.; Rao, R.; Luo, J.; Hudson, J.; Chen, J.; Rao, A. M. *Chem. Phys. Lett.* **2005**, *412*, 269−273.
(42) Kim, C.; Yang, K. S.; Kojima, M.; Yoshida, K.; Kim, Y. J.; Kim, Y. A.; Endo, M. *Adv. Funct. Mater.* **2006**, *16*, 2393−2397.

(43) Yao, J.; Wang, G. X.; Ahn, J. H.; Liu, H. K.; Dou, S. X. *J. Power Sources* **2003**, *114*, 292−297.
(44) Guo, P.; Song, H.; Chen, X. *Electrochem. Commun.* **2009**, *11*, 1320−1324.
(45) Zhang, S.; Shi, P. *Electrochim. Acta* **2004**, *49*, 1475−1482.